

A Two-Equation Subgrid Model for Large-Eddy Simulation of High Reynolds Number Flows

Yichuan Fang[#] and Suresh Menon^{*}

School of Aerospace Engineering
Georgia Institute of Technology, Atlanta, GA 30332

Abstract

A new two-equation Kinetic-Eddy Simulation (KES) model is developed for large-eddy simulation (LES) of wall-bounded high Reynolds number flows. This model solves for the local unresolved kinetic energy and the local length scale. The dissipation of the kinetic energy depends on the length scale, as well as, on the length scale gradient. New terms of subgrid viscous work, subgrid pressure diffusion, and subgrid heat transfer are also proposed for the closure of energy equation. In most of flow domain of simulated cases, the subgrid length scale is compatible to computational grid scale, and KES model behaves like a LES. In some other regions, the length scale tends toward the integral length scales, smoothly approaching very large-eddy simulation (VLES) limit. Thus, this closure is considered a VLES-LES approach. The KES model has been applied for 2D flows around NACA-0015 airfoils at different angles of attack, including regions of linear-lift, mild separation and static stall. The predicted aerodynamics compares well with experimental measurement. Especially in the static stall simulations, vortex shedding with massive separation is clearly captured.

I. Introduction

It is still one of the most challenging problems to accurately simulate high-Reynolds number turbulent flows around airfoils/wings at a large angle of attack (AoA). As summarized by Kotapati-Apparao *et al.* (2004), Mellen *et al.* (2003), and Dahlström and Davidson (2003), the flow includes adverse pressure gradient, streamline curvature, boundary layer separation, and transition from laminar to turbulent flow. There is also a flow singularity at the stagnation point at the airfoil leading edge (LE). The flow is sensitive to the airfoil geometry, the angle of attack, and the Reynolds number. Different flow regimes motivate various hierarchies of simulation strategies. In flows with a large AoA, the trailing edge (TE) separation is strongly coupled with the pressure peak at the leading edge. The wake is unsteady and complicated. Therefore all the regions around the airfoil are equally important. The object of this work is to investigate flows with mild and massive separation, and to investigate the feasibility of LES simulations for such flows.

Similar investigations have been performed in the European research project LESFOIL (see Mellen *et al.* 2003, for a detailed review). Several Reynolds-averaged Navier-Stokes (RANS) equation models (steady and unsteady, compressible and incompressible) were applied to the Aerospatiale A-airfoil at an angle of attack 13.3° . It was found that very few RANS models have the capability to resolve this problem accurately. Compared with experimental data, satisfying results were obtained by using compressible LES (Mary and Sagaut, 2002), incompressible LES (Dahlström and Davidson, 2003), and Detached-Eddy Simulation (Cokljat and Liu, 2002, and Kotapati-Apparao *et al.*, 2004).

Massively separated airfoil flows have a strong character of unsteadiness away from the wall. The RANS approaches, which are designed to solve the steady state, time-averaged flows, cannot be expected to predict this kind of turbulent flows well. Direct numerical simulation (DNS) would, of course, be the ideal method, if computational resource was available. LES is the current choice, which is an intermediate

[#] Postdoctoral Fellow, Member AIAA

^{*} Professor, AIAA Associate Fellow

technique between DNS and RANS. In LES, the contribution of the large, energy-containing structures to momentum and energy transfer is computed exactly, and only the effect of unresolved small scales of turbulence is modeled. Similar to DNS, LES has the capability to provide the time dependent flow features. However, LES is still extremely expensive, requiring fairly fine meshes in the near-wall region. In a wall-resolved LES, the distance from the wall to the first grid should be at least less than two wall units ($y_1^+ < 2$), in order to resolve the instantaneous velocity gradient close to the wall and capture the near-wall structures sufficiently (Piomelli and Chasnov, 1996). Thus, it is apparent that even a pure LES is nearly beyond current computer capacity for resolving wall turbulence at high Reynolds numbers. A natural way is to consider wall functions for LES with coarse grids (coarse LES), which allows the use of coarser resolution to reduce the cost for some specific flow cases (Mellen et al., 2003). But near-wall modeling for LES is not well understood (Piomelli and Balaras, 2002).

In this work, a new KES subgrid model is developed instead of a pure LES model, where two equations are solved for the subgrid kinetic energy and the subgrid length scales locally. Theoretically, KES becomes very large eddy simulation (VLES) when only the largest scales of turbulence are resolved on a very coarse grid; LES when small scales of turbulence close to grid are resolved; and direct numerical simulation (DNS) in the limit of very fine grid, i.e., the length scale and kinetic energy tend to vanish. KES is applicable to near-wall turbulence without any ad-hoc specification of the distance from the wall. This model has been applied to 2D flows around NACA-0015 airfoil. The numerical results have been compared with available experimental, and good agreement is observed.

II. Filtered Navier-Stokes Equations for LES

The equations governing the motion of the resolved eddies can be obtained by separating the large scales from the small scales. LES equations are obtained using a Favre (density weighted) spatial filtering of the compressible Navier-Stokes equations. A Favre-filtered variable is defined as $\tilde{f} = \overline{\rho f} / \bar{\rho}$. Applying the Favre-filtering operation, the resolved transport equations can be obtained in a conservative form as

$$\frac{\partial \bar{\rho}}{\partial t} + \frac{\partial}{\partial x_i} (\bar{\rho} \tilde{u}_i) = 0, \quad (2)$$

$$\frac{\partial \bar{\rho} \tilde{u}_j}{\partial t} + \frac{\partial}{\partial x_i} [\bar{\rho} \tilde{u}_i \tilde{u}_j + \bar{p} \delta_{ij} + \tilde{\tau}_{ij} + \tau_{ij}^{sgs}] = 0, \quad (3)$$

$$\frac{\partial \bar{\rho} \tilde{E}}{\partial t} + \frac{\partial}{\partial x_i} [(\bar{\rho} \tilde{E} + \bar{p}) \tilde{u}_i - \tilde{\tau}_{ij} \tilde{u}_j + \tilde{q}_i + E_i^{sgs} + p_i^{sgs} + \sigma_i^{sgs} + q_i^{sgs}] = 0, \quad (4)$$

where ρ is the density, u_i is the velocity in the x_i direction, p is the pressure, and $E (= e + \frac{1}{2} u_i^2)$ is the total energy per unit mass. The filtered total energy \tilde{E} includes the subgrid kinetic energy (to be discussed later) $k^{sgs} = \frac{1}{2} (\overline{u_i u_i} - \tilde{u}_i \tilde{u}_i)$ and is defined as

$$\tilde{E} = \tilde{e} + \frac{1}{2} \tilde{u}_i^2 + k^{sgs}. \quad (5)$$

Here the symbol “ $\overline{\leftarrow}$ ” represents the Favre filtering. The resolved molecular viscous stress and heat fluxes are given by

$$\tilde{\tau}_{ij} = 2\tilde{\mu}\tilde{S}_{ij} - \frac{2}{3}\tilde{\mu}\tilde{S}_{kk}\delta_{ij}, \quad \tilde{q}_i = -\tilde{\kappa}\frac{\partial \tilde{T}}{\partial x_i}, \quad (6)$$

where $\tilde{S}_{ij} = \frac{1}{2}(\partial \tilde{u}_i / \partial x_j + \partial \tilde{u}_j / \partial x_i)$ is the strain-rate tensor, and $\tilde{\mu}$ and $\tilde{\kappa}$ are the molecular viscosity and the thermal conductivity at the filtered temperature \tilde{T} , respectively. In the derivation, the molecular viscous stress is approximated as $\overline{\mu(T)S_{ij}} \approx \mu(\tilde{T})\tilde{S}_{ij}$.

The SGS effects appear through the SGS viscous stress τ_{ij}^{sgs} , SGS total energy diffusion E_i^{sgs} , SGS pressure diffusion P_i^{sgs} , SGS viscous diffusion σ_i^{sgs} , and SGS heat conduction q_i^{sgs} . These terms are unknown in the momentum and energy equations of the filtered Navier-Stokes, and are defined as,

$$\tau_{ij}^{sgs} = \overline{\rho(u_i u_j - \tilde{u}_i \tilde{u}_j)}, \quad (7)$$

$$E_i^{sgs} = \overline{\rho}(\overrightarrow{E}u_i - \tilde{E}\tilde{u}_i), \quad (8)$$

$$P_i^{sgs} = \overline{p}u_i - \tilde{p}\tilde{u}_i, \quad (9)$$

$$\sigma_i^{sgs} = \overrightarrow{\tau}_{ij}u_j - \tilde{\tau}_{ij}\tilde{u}_j, \quad (10)$$

$$q_i^{sgs} = \kappa(T)\frac{\partial T}{\partial x_i} - \tilde{\kappa}\frac{\partial \tilde{T}}{\partial x_i}. \quad (11)$$

III. KES Subgrid Model

KES momentum closure

Most SGS models currently used are the eddy-viscosity models (EVM) of the form

$$\tau_{ij}^{sgs} - \frac{1}{3}\tau_{kk}^{sgs}\delta_{ij} = -2\nu_t\tilde{S}_{ij} \quad (12)$$

that relates the SGS stresses τ_{ij}^{sgs} to the resolved strain-rate tensor \tilde{S}_{ij} through eddy viscosity ν_t . By dimensional analysis, the eddy viscosity ν_t is proportional to the product of SGS velocity scale, $\sqrt{k^{sgs}}$, and SGS length scale, l^{sgs} . Because the most active of the subgrid scales are those closest to the cutoff, the natural subgrid length scale in LES modeling is the filter length, which is proportional to the local grid size. In most applications, the eddy viscosity ν_t is obtained algebraically to avoid solving additional equations. For instance, in the most widely used Smagorinsky model (1963), it is assumed that the subgrid length scale is local grid spacing length ($l = \Delta$), and the eddy viscosity is written as $\nu_t = (C_s\Delta)^2|\tilde{S}|$, where $|\tilde{S}| = \sqrt{2\tilde{S}_{ij}\tilde{S}_{ij}}$ is the magnitude of the strain-rate tensor.

There are some other more accurate subgrid scale models, such as two-point closure models. Most of these models are based on the equilibrium hypothesis and was derived based on the theoretical analysis of energy transfer spectrum. But the spectral model is difficult to apply for complex turbulent flows, particularly in wall-bounded turbulence. In the presence of wall boundaries, the subgrid length scale needs to be modified to account for the reduced growth of the small scales near the wall. Usually the Van Driest damping function is introduced to modify the eddy viscosity. In the Detached-Eddy Simulation (DES) (Spalart et al. 1997), the normal wall distance is used to substitute the LES filter width for the pseudo-viscosity transport equation in the near-wall region.

In this work, a new approach is proposed. This model solves the subgrid k^{sgs} and $(kl)^{sgs}$ -equation for the subgrid velocity scale, $\sqrt{k^{sgs}}$, and the subgrid length scale, l^{sgs} . The transport equations for subgrid k^{sgs} and $(kl)^{sgs}$ are

$$\frac{\partial \overline{\rho}k^{sgs}}{\partial t} + \frac{\partial \overline{\rho}u_i k^{sgs}}{\partial x_i} = \tau_{ij}^{sgs} \frac{\partial \tilde{u}_i}{\partial x_j} - C_{\epsilon,k}\overline{\rho} \frac{(k^{sgs})^{3/2}}{l^{sgs}} + \frac{\partial}{\partial x_i} \left(\overline{\rho} \left(\frac{\nu}{Pr} + \frac{\nu_t}{\sigma_k} \right) \frac{\partial k^{sgs}}{\partial x_i} \right), \quad (13)$$

$$\frac{\partial \overline{\rho}(kl)^{sgs}}{\partial t} + \frac{\partial \overline{\rho}u_i (kl)^{sgs}}{\partial x_i} = C_l l^{sgs} \tau_{ij}^{sgs} \frac{\partial \tilde{u}_i}{\partial x_j} - C_{\epsilon,kl}\overline{\rho} (k^{sgs})^{3/2} + \frac{\partial}{\partial x_i} \left(\overline{\rho} \left(\frac{\nu}{Pr} + \frac{\nu_t}{\sigma_{kl}} \right) \frac{\partial (kl)^{sgs}}{\partial x_i} \right). \quad (14)$$

Here, the dissipation coefficient of $(kl)^{sgs}$ is a function of subgrid length gradient given as

$$C_{\epsilon,kl} = 0.58 + 2 \frac{C_\nu}{\sigma_{kl}} \left(\frac{\partial l^{sgs}}{\partial x_j} \right)^2. \quad (15)$$

The coefficient Pr is laminar Prandtl number, taken to be 0.72. The dissipation coefficient of subgrid k^{sgs} is $C_{\epsilon,k} = 0.916$, and the Prandtl-Schmidt number for subgrid k^{sgs} $\sigma_k = 0.9$. $C_\nu = 0.0667$ is the eddy viscosity coefficient. The production coefficient of subgrid $(kl)^{sgs}$ is $C_l = 1.06$, and the Prandtl-Schmidt number for subgrid $(kl)^{sgs}$ $\sigma_{kl} = 2$.

The subgrid-scale viscous stresses are modeled as a new approach,

$$\tau_{ij}^{sgs} = 2\bar{\rho}v_t[\tilde{S}_{ij} - \frac{1}{3}\tilde{S}_{kk}\delta_{ij}] - \frac{2}{3}\bar{\rho}k^{sgs}\delta_{ij} \quad (16)$$

with the subgrid eddy viscosity defined as

$$v_t = C_v(k^{sgs})^{1/2}l^{sgs} \quad (17)$$

Here, the length scale, l^{sgs} , is a natural scale to bridge LES with DNS and VLES. Theoretically, when the length scale, l^{sgs} , is close to the computational grid size Δ , it approaches LES; when the computational grid size Δ becomes as small as to Kolmogorov length scale, the subgrid length scale l^{sgs} should vanish in the limit of DNS; when the length scale, l^{sgs} , becomes much larger than Δ , then it approaches the integral length scale and becomes very large-eddy simulation (VLES). These limiting features still need to be proven and full evaluation of the KES approach is planned in the near future to properly validate and establish this methodology. Also note that since l^{sgs} is a continuous function, there will be regions where this model will predict neither LES nor VLES. The performance of KES in this intermediate region is of particular interest in this study.

KES energy transport closure

In addition to the closure for τ_{ij}^{sgs} of equation (7), there are other unclosed terms appearing in the LES filtered energy equation. In this work, SGS total energy E_i^{sgs} , SGS pressure diffusion P_i^{sgs} , SGS viscous work σ_i^{sgs} , and SGS heat conduction q_i^{sgs} are explicitly closed as,

$$E_i^{sgs} = -\frac{\bar{\rho}v_t}{\sigma_e} \frac{\partial \tilde{E}}{\partial x_i}, \quad (18)$$

$$P_i^{sgs} = -\frac{\bar{\rho}v_t}{\sigma_p} \frac{\partial \tilde{P}}{\partial x_i}, \quad (19)$$

$$\sigma_i^{sgs} = -\tau_{ij}^{sgs} \tilde{u}_j, \quad (20)$$

$$q_i^{sgs} = -\frac{\bar{\rho}v_t C_p}{\sigma_t} \frac{\partial \tilde{T}}{\partial x_i}, \quad (21)$$

where σ_e , σ_p and σ_t are the effective subgrid Prandtl-Schmidt numbers for energy, pressure, and temperature, respectively. At present they are taken as 0.9.

KES realizability

In principle, the realizability conditions of LES should be constrained as, $\bar{\rho}(\overleftarrow{u_i u_i} - \tilde{u}_i \tilde{u}_i) \geq 0$, $(\bar{\rho} \overleftarrow{u_i u_j} - \bar{\rho} \tilde{u}_i \tilde{u}_j)^2 \leq (\bar{\rho} \overleftarrow{u_i u_i} - \bar{\rho} \tilde{u}_i \tilde{u}_i)(\bar{\rho} \overleftarrow{u_j u_j} - \bar{\rho} \tilde{u}_j \tilde{u}_j)$, and $\det(\bar{\rho} \overleftarrow{u_i u_j} - \bar{\rho} \tilde{u}_i \tilde{u}_j) \geq 0$ in an eddy viscosity model (EVM). Earlier, k^{sgs} based one-equation LES subgrid model was observed to satisfy all these realizability constraints (Nelson and Menon, 1998). At present, these constraints have not been strictly enforced for the KES model. Rather, a lower limit for k^{sgs} and l^{sgs} (for instance, 10^{-23} is used in KES) are enforced. For the subgrid length scale, l^{sgs} , the upper limit should tend toward the integral scale, which is determined by geometrical considerations. $l^{sgs} / \Delta \leq 200$ is employed for the present study. Future studies will revisit these limiting values and the realizability constraints.

The class of k-equation models is known to overproduce production in the region near a stagnation point, known as the *stagnation point anomaly* (Durbin and Petterson, 2001). This can be improved by, following Durbin's correction (Durbin, 1996), by using the realizability constraint, $0 \leq \tau_{ij}^{sgs} \leq 2k^{sgs}$, upon the eddy viscosity via a bound on the time scale. The subgrid viscosity is modified with a bounding viscosity $v_{t,max}$ as

$$v_t = \min(v_t, v_{t,\max}), \quad v_{t,\max} = \frac{k^{sgs}}{\sqrt{6\tilde{S}_{ij}\tilde{S}_{ij}}} \quad (22)$$

Again, these limiting constraints are defined for the particular application of external flow studies. The generality of this approach or its validity for other applications remains to be established.

IV. Numerical Approach

The LES filtered equations along with the KES subgrid model equations (13-14) are integrated by a dual time-stepping procedure (Jameson, 1991) and discretized by the finite volume method (FVM) in this work. A second-order accurate, three-point backward differencing is used in the physical time discretization, and the modified five-stage Runge-Kutta scheme (Jameson, et al., 1981; Jameson, 1991) is implemented for the pseudo-time evolution of solutions between the physical time steps. A cell-centered second-order scheme is applied in the space discretization. In order to eliminate spurious fluctuations, the second and fourth-order Jameson artificial dissipation (Jameson, 1991), based on pressure gradient, is applied. The viscous coefficients of 0.01 and 0.008 are employed for the second and fourth-order dissipation.

The far-field characteristic boundary condition (Jameson, 1985) is specified at the outer boundary of the C-grid by computing one dimensional Riemann invariants. At the outflow boundary, zero gradient condition is generally applied for the flow variables. At the wall, the no-slip condition is used with zero-gradient for pressure and adiabatic wall for temperature. In the spanwise direction, periodic boundary conditions are employed.

Both of k^{sgs} and l^{sgs} are set to zero on the wall. Based on the analyses of energy dissipation rate on the wall, the following values are imposed on the first cells above the surface,

$$k^{sgs} = 0.25\nu(\tilde{u}_i\tilde{u}_i)^{0.5} / \Delta_1 \quad (23)$$

$$l^{sgs} = \sqrt{k^{sgs}} \Delta_1^2 / (0.53\nu) \quad (24)$$

where Δ_1 is the grid length scale of the first cells, and ν the kinematic viscosity. This set of condition, equations (23) and (24), has been tested for $y_1^+ < 5$ in this work. k^{sgs} is set to $(0.016u_\infty)^2$ and l^{sgs} is set to the local grid length scale Δ at far field, and they are initialized with the same corresponding value also.

An efficient parallel version of the solver has been developed, based the Message-Passing Interface (MPI) library. For the parallelization and complex geometry applications, the computational domain is split into multi-blocks, and each block is decomposed into zones. Each zone is enclosed with up to three layers of ghost cells. The ghost cells store flow variables transferred from the neighboring zone as numerical boundary condition. The parallel code has been tested on different system with good parallel efficiency.

V. Results and Discussion

In this section, the numerical results of KES for the 2D flow around a NACA-0015 airfoil are presented at different angles of attack. Lift region covers the linear-lift, static stall, and mild separation in between. The model behavior of KES is studied in detail in the static stall region. The free stream Mach number is 0.291, and Reynolds number based on the free stream velocity, u_∞ , and airfoil chord, C , is about 2×10^6 . The flow condition is setup according to the experiment of Piziali (1994). A multiblock of C-grid is used for the space discretization, as shown in Figure 1, where wake zone is cut into two blocks along the airfoil chord at the trailing edge. The outer boundary is set approximately $8C$. The normal distance of the first grids to the wall is $y_1 / C = 1 \times 10^{-5}$, with $y_1^+ < 5$. The spanwise distance is $z / C = 0.0012$. The grid size is $541 \times 97 \times 2$, which includes 391 points around the airfoil and 75 points in the wake.

Although all studies represented here are for 2D, it is well understood that VLES/LES studies must be performed in full 3D to recover realistic turbulence dynamics. The results reported here are the first evaluations of this model. 3D simulations are underway and will be reported in the near future.

Attached flows around NACA0015 airfoil

The 2D attached flow around NACA0015 at AoA = 0° is simulated first. As shown in the instantaneous streamlines of Figure 2(a), no separation is observed. Figure 2(b) shows the pressure coefficient distribution, in an excellent agreement with experimental measurement.

In the flow around NACA-0015 at AoA =13° there is mild separation near the trailing edge, as shown in Figure 3(a) by the streamlines of time-averaged flow. In the simulation of eight flow-time cycles, there is no significant difference between the instantaneous and time-averaged flow field for the flow streamlines, and the distribution of pressure and surface friction along the airfoil. Figure 3(b) shows that the time-averaged pressure coefficient C_p of KES agrees well with experimental data.

Static stall around NACA0015 airfoil

The flow around NACA0015 separates massively at angles of attack after 16°, and static stall happens. In this region, the flow has a strong character of unsteadiness. It is a big challenge to regular RANS models. KES is a model between LES and RANS, which is expected to capture turbulence structures near the wall at a grid resolution of RANS and capture unsteady phenomenon at the limit of LES. The flows at AoA = 16° and 17° are fully separated. Such simulations are a good test case to check the model behavior and performance.

In the simulation of case with AoA=16°, the flow is averaged for about eight flow-time cycles after transition from initial condition. Figure 4(a) presents the time averaged streamlines. It can be seen that a big separation bubble exists near the trailing edge, which covers almost 2/3 of the airfoil upper surfaces. The predicted pressure coefficient agrees very well with experimental measurement, as represented by the black solid line in Figure 4(b). In Figure 4(b), the green dash is the distribution of an instantaneous pressure coefficient. It varies with the movement of vortex shedding from suction region and trailing edge. The unsteady movement of vortices is shown by the instantaneous streamlines in Figure 5. From the instantaneous streamlines it is seen that the flow is stalled with massive separation on the airfoil. At the earlier time, $T1=1.3 \times 10^{-2}$ sec, one large-scale vortex originates around each of the suction region and trailing edge, rotating in opponent directions. In between, there is a larger vortex, which rotates in the same direction as the one from the suction region. The suction region vortex moves downstream and merges into the large vortex. The large vortex attracts the trailing edge vortex, and eventually is shed into the wake when becoming strong enough to leave the airfoil.

Figure 6 shows the subgrid kinetic energy k^{sgs} contours at time $T2=2.5 \times 10^{-2}$ sec. In such separated flows, the estimated k^{sgs} by KES has a strong feature of unsteadiness. The averaged Reynolds stresses are shown in Figure 7. As shown in Figure 7(a), both of areas near the trailing edge and suction region, where vortex is shed from, have a high value of u_{rms} . However, v_{rms} is strong only in the wake region right after the trailing edge, as shown in Figure 7(b). Similar to u_{rms} the antisymmetric stresses $\langle u'v' \rangle$ is more active in the suction region, as shown in Figure 7(c). From the contours of Reynolds stresses, it can be seen that turbulence dominates in both suction region and trailing edge.

Figures 8(a-c) show the ratio of subgrid length scale to grid length scale, l^{sgs} / Δ , for cases with AoA = 0°, 13° and 16°, respectively. In Figure 8(a), the vortex shear is not strong near the suction region. The ratio, l^{sgs} / Δ , is smooth all over the flow field, except that high values exist in the leading edge and trailing edge. It is common in all simulation. The increase of length scale might be due to the singularity at the leading and trailing edge. In Figure 8(b) with AoA = 13°, there are several points of oscillation in the region above the trailing edge, where shear is strong. In Figure 8(c) with AoA = 16°, the oscillation points with high value of the ratio move upstream to the suction region, where shear becomes strong. Over all, the ratio of l^{sgs} / Δ becomes bigger in AoA 16° than that in AoA 13° wherever shear is stronger.

The energy dissipation is also adjusted based on the variation of the subgrid length scale. Figures 9(a-c) show the length scale l^{sgs} , for the three AoA cases, in order to compare the pattern of l^{sgs} / Δ shown in Figures 8(a-c). In the wake region and wall boundary layer, the l^{sgs} is small. It also increases with turbulence diffusing downstream in the wake. Figure 9(c) shows that the l^{sgs} follows the vortex pattern in the recirculation zone and the wake. Comparing Figures 8(c) and 9(c), it can be seen that l^{sgs} / Δ depend on both grid resolution and vortex structure in the flow. Model equation (15) also shows that the dissipation of

subgrid length scale changes with the gradient of subgrid length scale l^{sgs} . In most of other region with relatively weaker shear, the subgrid length l^{sgs} has a value comparable to the grid length scale Δ . The behavior of l^{sgs} / Δ and l^{sgs} makes KES a multiscale model and behave as a LES in most of the flow region.

Figures 10(a-e) show instantaneous vorticity around NACA0015 at AoA = 17° at five time instants. It covers almost one cycle of vortex shedding from the trailing edge from 8.4×10^{-3} s to 1.7×10^{-2} s. The corresponding k^{sgs} contours are also shown in Figures 11(a-e), respectively. It can be seen that k^{sgs} contours closely flow the vortex shedding, which is as expected. Figure 12 shows the pressure coefficient distribution of time averaged flow at AoA 17°, in a good agreement with experiment. In the region near the trailing edge, the pressure is overpredicted by KES. It might be owing to the 2D nature of current study.

Airload Analysis

In the experiment (Peziali, 1994), the airfoil pitched at frequency which is low enough to be looked at as a static stall. The airload prediction around NACA0015 airfoil has been carried out in ONERA (Gleize, *et al.* 2004) using various RANS models of Spalart-Allmaras, k- ω , k- ω with SST correction, k- ω with Kok modification, k- ω Kok + SST, k-l, k- ϵ , and multi-scale model. In the ONERA study, lift coefficient C_L was overpredicted and drag coefficient C_D was underpredicted after static stall, even with fine grids up to 3.5 million. As shown in Figure 14, current KES results of C_L , C_D , and moment coefficient C_M agree well with experiment. Especially, the values of C_L , C_D and C_M are in the middle of the range between up-stroke and down-stroke after static stall in simulated cases with AoA up to 17°. The aerodynamics before static stall is taken from an instant flow when the flow solution converges to a steady state. For both cases with AoA = 13° and 16°, the airload is obtained with a time-averaged solution of about eight flow-time cycles. For the case with AoA = 17°, about 5.6 flow-time cycles of flow are averaged.

V. Concluding Remarks

A two-equation subgrid model is developed for application to high Reynolds, wall bounded flows. This model solves for both the characteristic unresolved kinetic energy and the local length scale. It also does not require any specification of distance from the wall, as needed in other hybrid RANS-LES approach. This model has been applied to 2D flows around NACA-0015 airfoil at different angles of attack, including region of linear-lift, mild separation and static stall. The predicted aerodynamics agrees well with available experimental data, especially for the airload. This model is successfully in predicting the static stall with satisfying accuracy, and has the capability to capture vortex shedding and massive separation at high Reynolds number. In the future, a dynamic model for the coefficients of eddy viscosity and kinetic energy dissipation will be developed. Many issues still remain to be addressed. The current simulations were limited to 2D due to resource constraint. Full 3D simulations are underway and need to be analyzed. The realizability constraints and the limiting behavior of the KES model need to be addressed not only for airfoil flows, but also for more canonical flows such as isotropic turbulence and spatial shear layers. Finally a locally dynamic model for the estimation of model constants is being developed based on earlier work (Kim and Menon, 1999). This model will be needed to give general universality to the KES approach.

Reference:

1. Cokljat, D. and Liu, F., "DES of Turbulence Flow over an Airfoil at High Incidence," AIAA Paper 2002-0590, 2002.
2. Dahlström, S. and Davidson, L., "Large-Eddy Simulation Applied to a High-Reynolds Flow around an Airflow Close to Stall," AIAA Paper 2003-0776, 2003.
3. Durbin, P.A. and Petterson Reif, B.A., *Statistical Theory and Modeling for Turbulent Flows*, pp. 136-138, John Wiley & Sons, LTD, 2001.
4. Durbin, P.A., "On the k- ϵ stagnation point anomaly," *International Journal of Heat and Fluid Flow*, Vo. 17, pp. 89-90, 1996.
5. Fureby, C. and Möller, S.-I., "Large-Eddy Simulation of Reacting Flows Applied to Bluff Body Stabilized Flames," *AIAA Journal*, Vol. 33, No. 12, pp. 2339-2347, 1995.

6. Jameson, A., "Time Dependent Calculations Using Multigrid, with Applications to Unsteady Flows Past Airfoils and Wings," AIAA Paper 91-1596, 1991.
7. Jameson, A., "Transonic Flow Calculations," in *Numerical Methods in Fluid Dynamics*, edited by F. Brezzi, Lecture Notes in Mathematics, Vol. 1127, pp. 156-242, Springer-Verlag, 1985.
8. Jameson, A., Schmidt, W. and Turkel, E., "Numerical Solution of the Euler Equations by Finite Volume Methods using Runge-Kutta Time-Stepping Schemes," AIAA Paper 81-1259, 1981.
9. Kim, W.W. and Menon, S., "A New Incompressible Solver for Large-Eddy Simulation," *International Journal of Numerical Fluid Mechanics*, Vol. 31, pp. 983-1017, 1999.
10. Kotapati-Apparao, R.B., Squires, R.B. and Forsythe, R.B., "Prediction of the Flow over an Airfoil at Maximum Lift," AIAA Paper 2004-0259, 2004.
11. Leonard, A., "Energy Cascade in Large-Eddy Simulations of Turbulent Fluid Flow," *Adv. Geophys.*, Vol. 18A, pp. 237-248, 1974.
12. Mary, I. and Sagaut, P., "Large Eddy Simulation of Flow around an Airfoil near Stall," *AIAA Journal*, Vol. 40, No. 6, 2002.
13. Mellen, C.P., Fröhlich, J. and Rodi, W., "Lessons from LESFOIL Project on Large-Eddy Simulation of Flow around an Airfoil," *AIAA Journal*, Vol. 41, No. 4, 2003.
14. Menon, S., Stone, C. and Patel, N., "Multi-Scale Modeling for LES of Engineering Designs of Large-Scale Combustors," AIAA Paper 2004-0157, 2004.
15. Piomelli, U. and Balaras, E., "Wall-Layer Models for Large-Eddy Simulations," *Annu. Rev. Fluid. Mech.* Vol. 34, pp. 349-74, 2002.
16. Piomelli, U. and Chasnov, J.R., "Large-Eddy Simulations: Theory and Applications," in Henningson, D., Hallböck, M., Alfredsson, H. and Johansson, A., *Transition and Turbulence Modeling*, pp. 269-336, Dordrecht, Kluwer Academic Publishers, 1996.
17. Smagorinsky, J., "General Circulation Experiments with the Primitive Equations, I. The Basic Experiment," *Monthly Weather Review*, Vol. 91, pp. 99, 1963.
18. Spalart, P.R. and Allmaras, S.R., "A One-Equation Turbulence model for Aerodynamic Flow," *La Recherche Aerospaciale*, Vol.1, pp. 5-21, 1994.
19. Spalart, P.R., Jou, W-H., Strelets, M. and Allmaras, S.R., "Comments on the Feasibility of LES for Wings, and on the Hybrid RANS/LES Approach," in *Advances in DNS/LES*, 1st AFOSR Int. Conf. on DNS/LES, Greyden Press, Columbus Oh, Aug. 4-8, 1997.
20. Yoshizawa, A. "Statistical Theory for Compressible Turbulent Shear Flows, with the Application to Subgrid Modeling," *Physics of Fluids A*, Vol. 29, pp. 2152-2164, 1986.
21. Arunajatesan, S., Sinha, N., and Menon, S., "Towards Hybrid LES-RANS Computations of Cavity Flowfields," AIAA Paper 2000-0401, 2000.
22. Speziale, C. G., "A Combined Large-Eddy Simulation and Time-Dependent RANS Capability for High-Speed Compressible Flows," *Journal of Scientific Computing*, Vol. 13, 1998.
23. Piziali, R.A., "2-D and 3-D Oscillating Wing Aerodynamics for a Range of Angle of Attack Including Stall," NASA-TM-4632, September 1994.

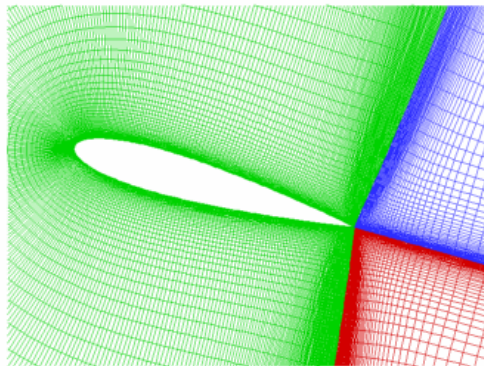


Figure 1. Multiblock C-grid around NACA-0015 airfoil

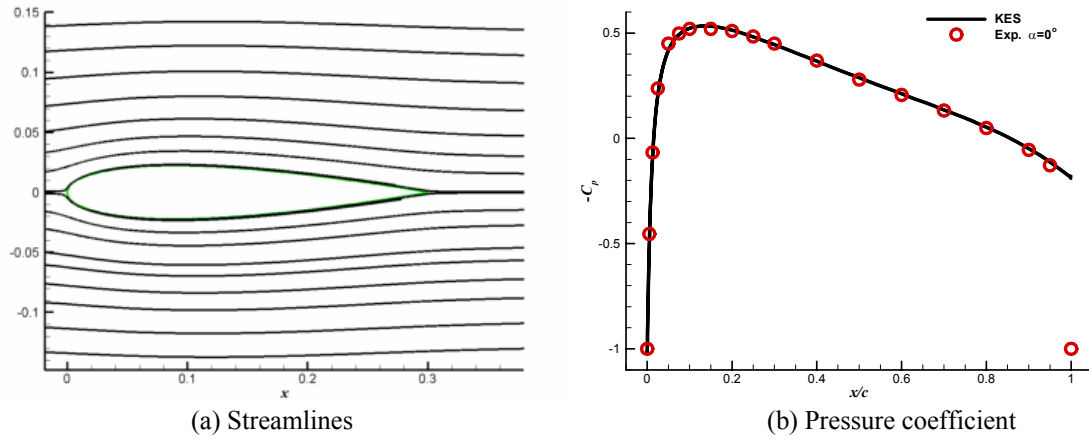


Figure 2. Streamlines and pressure coefficient around NACA0015 airfoil. $\text{AoA} = 0^\circ$.

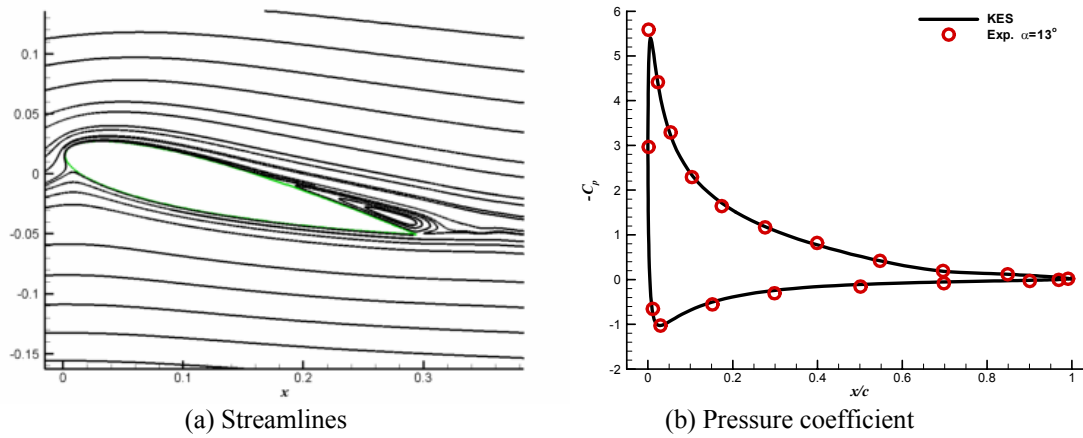


Figure 3. Streamlines and pressure coefficient of the time-averaged flow around NACA0015 airfoil. $\text{AoA} = 13^\circ$.

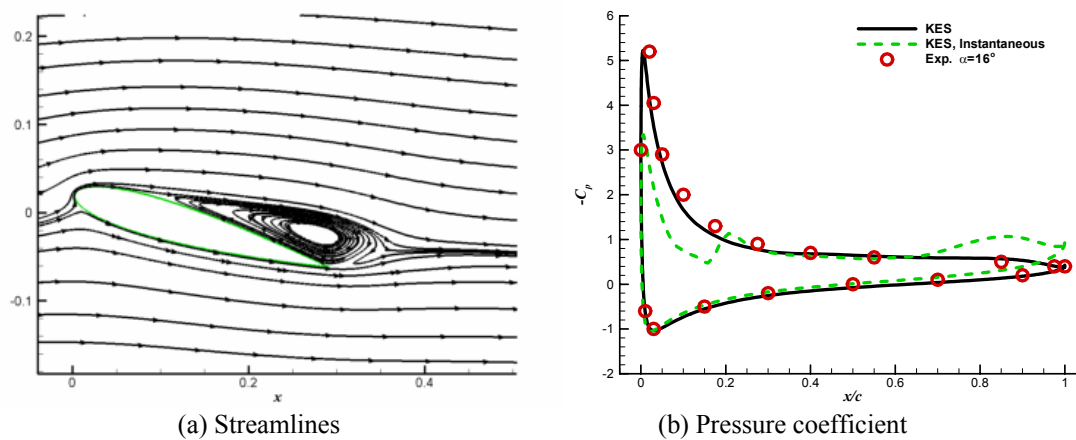


Figure 4. Streamlines and pressure coefficient of the time-averaged flow around NACA0015 airfoil. $\text{AoA} = 16^\circ$.

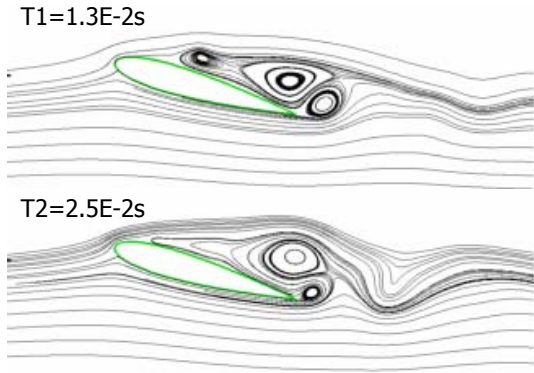


Figure 5. Instantaneous streamlines around NACA0015 airfoil at different time. AoA=16°.

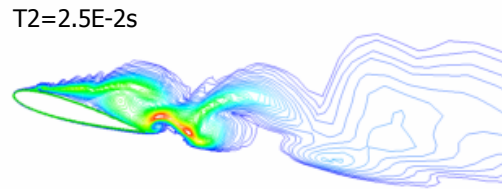
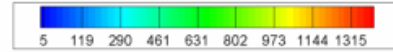
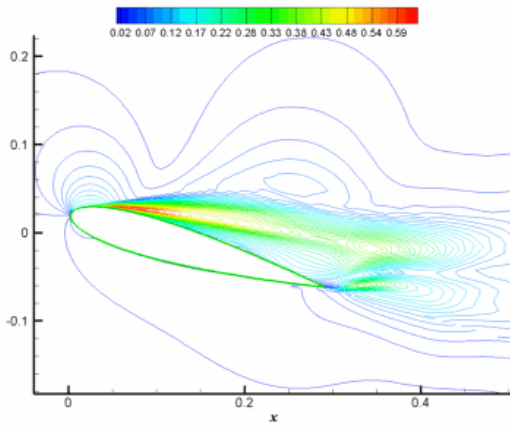
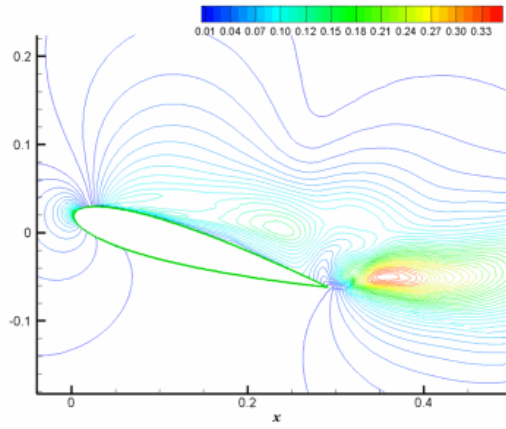


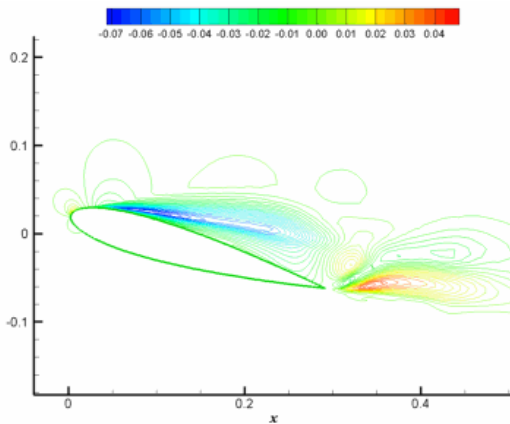
Figure 6 Instantaneous subgrid k^{sgs} around NACA0015 airfoil. AoA=16°.



(7a) u_{rms} / u_{∞}

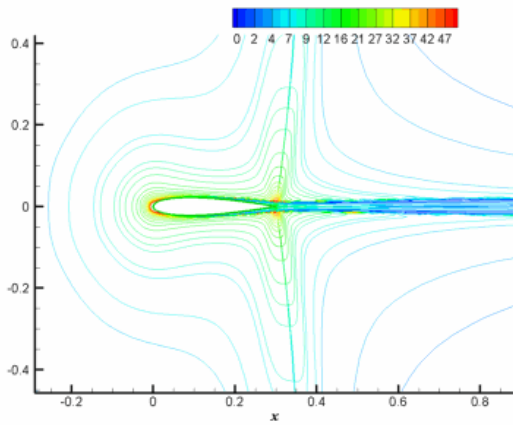


(7b) v_{rms} / u_{∞}

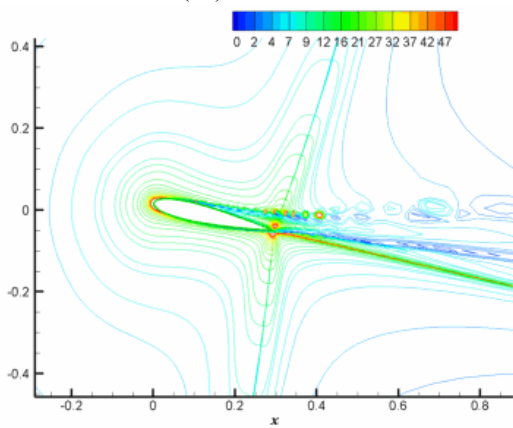


(7c) $\langle u'v' \rangle / u_{\infty}^2$

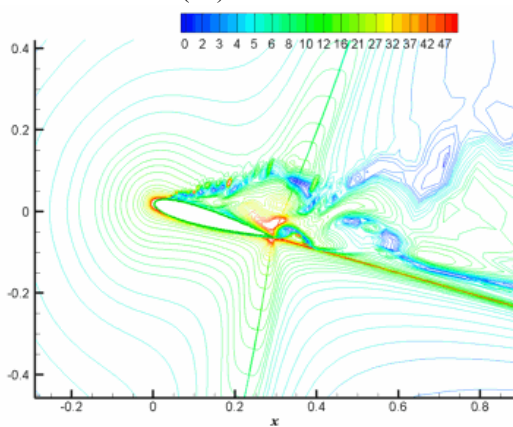
Figure 7. Contours of time-averaged Reynolds stress around NACA0015 airfoil. (a): u_{rms} / u_{∞} ; (b): v_{rms} / u_{∞} ; (c): $\langle u'v' \rangle / u_{\infty}^2$.



(8a) AoA = 0°

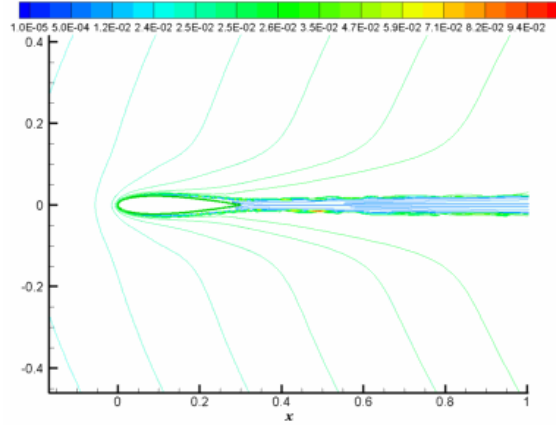


(8b) AoA = 13°

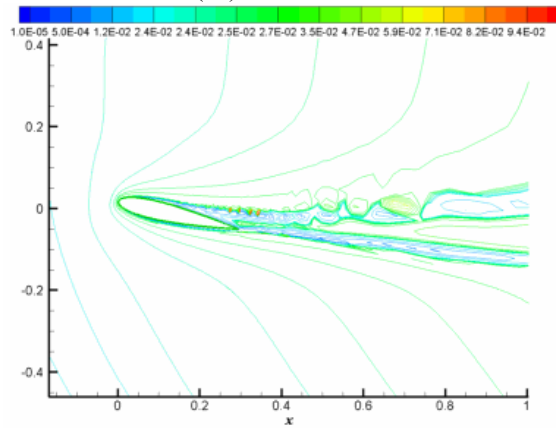


(8c) AoA = 16°

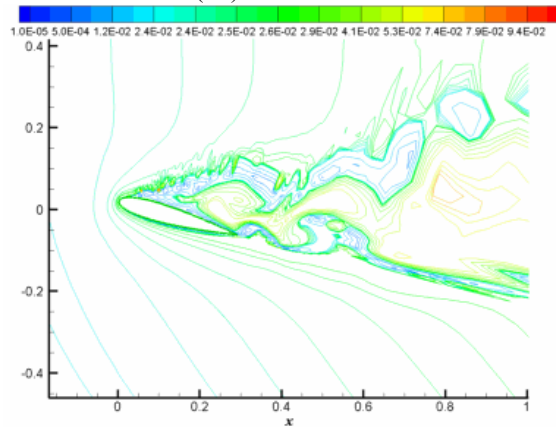
Figure 8. Contours of instantaneous l^{sgs} / Δ around NACA0015 airfoil. (a): 0°; (b): 13°; (c): 16° .



(9a) AoA = 0°



(9b) AoA = 13°



(9c) AoA = 16°

Figure 9. Contours of instantaneous l^{sgs} around NACA0015 airfoil. (a): 0°; (b): 13°; (c): 16° .

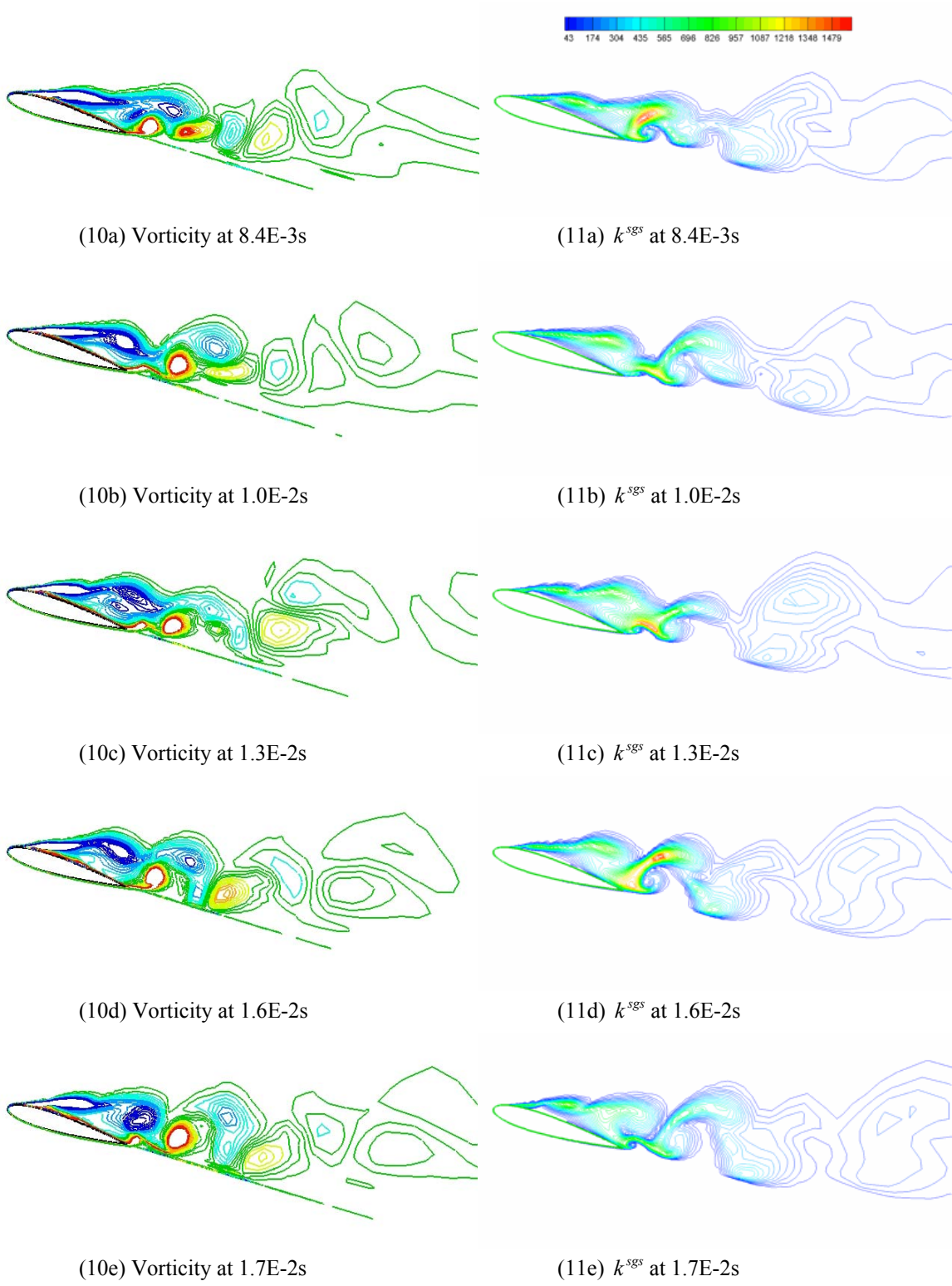


Figure 10. Snapshot of instantaneous vorticity around NACA0015 airfoil, AoA = 17°.

Figure 11. Snapshot of instantaneous subgrid k^{sgs} around NACA0015 airfoil. AoA=17°.

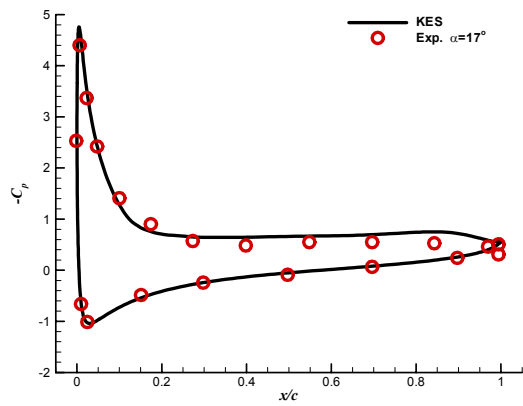
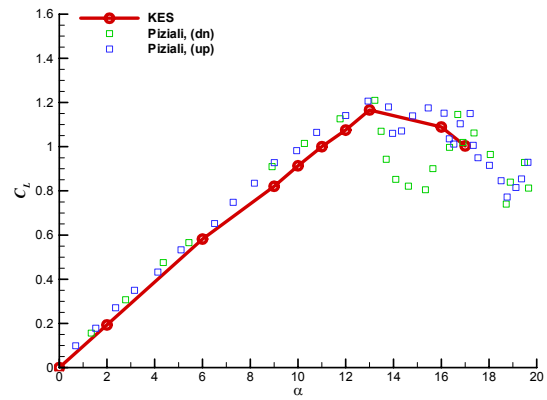
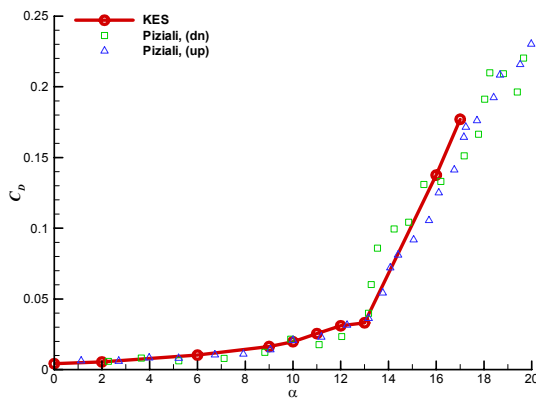


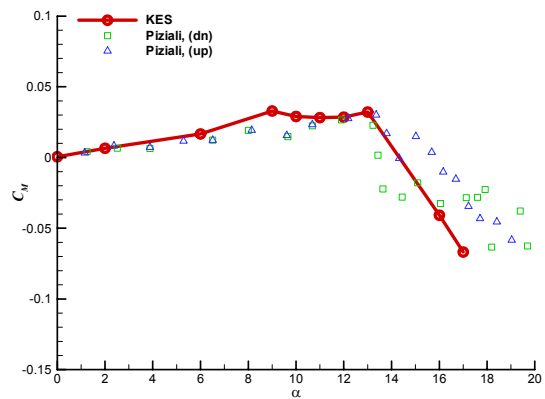
Figure 12. Pressure coefficient around NACA0015 airfoil. $\text{AoA} = 17^\circ$.



13(a) Lift coefficient



13(b) Drag coefficient.



13(c) Moment coefficient

Figure 13. Comparison of KES and experiment (Piziali, 1994) for the airloads around NACA0015 airfoil. (a): Lift coefficient; (b): Drag coefficient; (c): Moment coefficient.